

# Boxes, Boosts, and Energy Duality: Understanding the Galactic-Center Gamma-Ray Excess through Dynamical Dark Matter

Kimberly K. Boddy<sup>1\*</sup>, Keith R. Dienes<sup>2,3†</sup>, Doojin Kim<sup>4,5‡</sup>,  
Jason Kumar<sup>1§</sup>, Jong-Chul Park<sup>6¶</sup>, Brooks Thomas<sup>7\*\*</sup>

<sup>1</sup> *Department of Physics & Astronomy, University of Hawaii, Honolulu, HI 96822 USA*

<sup>2</sup> *Department of Physics, University of Arizona, Tucson, AZ 85721 USA*

<sup>3</sup> *Department of Physics, University of Maryland, College Park, MD 20742 USA*

<sup>4</sup> *Department of Physics, University of Florida, Gainesville, FL 32611 USA*

<sup>5</sup> *Theory Division, CERN, CH-1211 Geneva 23, Switzerland*

<sup>6</sup> *Department of Physics, Chungnam National University, Daejeon 34134 Korea*

<sup>7</sup> *Department of Physics, Lafayette College, Easton, PA 18042 USA*

Many models currently exist which attempt to interpret the excess of gamma rays emanating from the Galactic Center in terms of annihilating or decaying dark matter. These models typically exhibit a variety of complicated cascade mechanisms for photon production, leading to a non-trivial kinematics which obscures the physics of the underlying dark sector. In this paper, by contrast, we observe that the spectrum of the gamma-ray excess may actually exhibit an intriguing “energy-duality” invariance under  $E_\gamma \rightarrow E_*^2/E_\gamma$  for some  $E_*$ . As we shall discuss, such an energy duality points back to a remarkably simple alternative kinematics which in turn is realized naturally within the Dynamical Dark Matter framework. Observation of this energy duality could therefore provide considerable information about the properties of the dark sector from which the Galactic-Center gamma-ray excess might arise, and highlights the importance of acquiring more complete data for the Galactic-Center excess in the energy range around 1 GeV.

## I. INTRODUCTION

A robust excess in the flux of gamma-ray photons emanating from the Galactic Center (GC) with energies of  $\mathcal{O}(\text{GeV})$  has been observed in Fermi Large Area Telescope (Fermi-LAT) data. This excess was first noted in Ref. [1] and corroborated by a number of subsequent, independent analyses [2–13], including a dedicated study by the Fermi-LAT collaboration itself [14]. This excess consists not of a spectral line, but rather of a continuum bump which extends over a range of photon energies  $0.3 \text{ GeV} \lesssim E_\gamma \lesssim 50 \text{ GeV}$  and peaks at approximately  $E_\gamma \sim 1 \text{ GeV}$ .

A variety of possible explanations have been advanced as to the origin of this gamma-ray excess. Possible astrophysical explanations include emission from a population of millisecond pulsars [2–4, 6, 8, 15] and the decay of neutral pions produced by collisions of cosmic-ray particles with interstellar gas [2–4, 6]. However, the spectrum produced by millisecond pulsars is too soft in the sub-GeV region to explain the observed data [16] and millisecond pulsars born in globular clusters can account for only a few percent or less of the observed excess [17].

In addition, the observed distributions of gas seem to yield a poor fit to the spatial distribution of the signal [10, 18, 19]. More recently, in Refs. [20, 21], it has been asserted that the excess can be described by a set of unresolved point sources, and new methods to characterize these sources were devised.

An exciting alternative possibility is that the excess is the result of annihilating or decaying dark-matter particles within the galactic halo. Indeed, the spatial morphology of the excess is consistent with dark-matter annihilations from a spherically symmetric density profile, and the excess extends outward more than  $10^\circ$  from its center at the dynamical center of the Milky Way [9]. As a result, a variety of models currently exist in the literature which posit a dark-matter origin for the continuum feature observed in the Fermi-LAT data.

In such models, a suitably broad spectrum of gamma rays is realized through a variety of complicated cascade mechanisms. For example, such a gamma-ray spectrum can be generated via the subsequent showering and/or hadronization of Standard-Model (SM) particles initially produced directly from dark-matter annihilation. The observed excess is well reproduced by a dark-matter (DM) particle with a mass  $m_\chi \sim (30 - 50) \text{ GeV}$  and an annihilation cross-section  $\langle\sigma v\rangle \approx (1 - 3) \times 10^{-26} \text{ cm}^3/\text{s}$  which annihilates primarily to  $b\bar{b}$  [9, 13]. Likewise, a dark-matter particle with a mass  $m_\chi \sim 10 \text{ GeV}$  and an annihilation cross-section  $\langle\sigma v\rangle \approx (0.5 - 2) \times 10^{-26} \text{ cm}^3/\text{s}$  which annihilates primarily to  $\ell^+\ell^-$  [10] also provides a good fit to the Fermi-LAT data, provided that secondary photons produced by inverse Compton scattering and bremsstrahlung processes involving both primary

\*E-mail address: kboddy@hawaii.edu

†E-mail address: dienes@email.arizona.edu

‡E-mail address: doojin.kim@cern.ch

§E-mail address: jkumar@hawaii.edu

¶E-mail address: jcpark@cnu.ac.kr

\*\*E-mail address: thomasbd@lafayette.edu

and secondary electrons are taken into account. On the other hand, the recent AMS-02 data on the cosmic-ray antiproton flux [22, 23] has begun to exclude states in which a  $q\bar{q}$  final state dominates [24]. Concrete models in which the dark-matter candidate annihilates primarily to  $b\bar{b}$  [25–30] and to  $\ell^+\ell^-$  [31, 32] have also been identified. Indeed, additional studies on other final states [13] and generic model constraints [33] have established that there exist further SM channels through which a dark-matter particle can annihilate or decay and reproduce the observed excess. Cascades involving one or more exotic intermediary particles which eventually decay down to SM fermions which in turn subsequently shower or hadronize have also been considered [34–38].

While dark-matter models of this sort are capable of reproducing the GC excess, the showering and cascade dynamics on which these models rely in order to generate an acceptable gamma-ray spectrum have their disadvantages as well. For example, their complicated dynamics obscures the relationship between the detailed shape of the gamma-ray spectrum and the properties of the underlying dark sector.

In this paper, by contrast, we propose a set of models in which the kinematics connecting the gamma-ray spectrum back to the dark sector is more straightforward. As a result, we find that characteristic imprints in the shape of that spectrum can potentially provide direct information about the dark sector.

We begin our study by identifying a characteristic feature of the GC gamma-ray excess which points back to a particularly simple photon-production kinematics. In particular, we observe that the spectrum of this excess may potentially exhibit an intriguing “energy duality” under which the spectrum remains invariant under the transformation  $E_\gamma \rightarrow E_*^2/E_\gamma$  for some self-dual energy  $E_*$ . As we shall argue, the presence of such an energy duality is indicative of a particularly simple kinematics in which the signal photons are produced directly via the two-body decays of an intermediary particle.

Energy dualities of this sort have been exploited in other contexts involving similar decay kinematics, such as cosmic-ray pion decay [39] and the decay of heavy (new) particles produced at colliders [40]. At present, due to uncertainties in the astrophysical modeling of the GC region and also due to a paucity of reliable information about the shape of the spectrum at photon energies  $\mathcal{O}(10 \text{ MeV}) \lesssim E_\gamma \lesssim \mathcal{O}(1 \text{ GeV})$ , the information contained in the Fermi-LAT data alone is not sufficient to conclusively determine whether the spectrum of the GC excess in fact displays such an energy duality. Nevertheless, as we shall discuss, if such a duality *were* to be confirmed through future experiments, this result would immediately favor a particular class of dark-matter models. Moreover, these observations apply not only for the GC gamma-ray spectrum but also for the spectra from other sources, such as dwarf galaxies, for which backgrounds can be more reliably estimated.

While a spectrum with these duality properties can be

realized in certain cascade-based models [41], we shall show that a self-dual gamma-ray spectrum also has a natural interpretation within the Dynamical Dark Matter (DDM) framework [42, 43]. Indeed, as we shall show, there exists a simple class of DDM models which yield an energy-dual spectrum that provides an excellent fit to the Fermi-LAT data, with a self-dual energy  $E_* \sim \mathcal{O}(1 \text{ GeV})$ . These results further highlight the importance of acquiring more complete gamma-ray data in the energy range  $10 \text{ MeV} \lesssim E_\gamma \lesssim 1 \text{ GeV}$ .

This paper is organized as follows. In Sect. II, we examine the energy spectrum of the GC excess and discuss the extent to which it might potentially exhibit an energy-duality invariance under  $E_\gamma \rightarrow E_*^2/E_\gamma$  with  $E_* \sim \mathcal{O}(1 \text{ GeV})$ . In Sect. III, we then discuss how a gamma-ray spectrum with such an invariance can arise from dark-matter annihilation or decay. In Sect. IV, we introduce a series of simple DDM models which give rise to a gamma-ray spectrum with this invariance and demonstrate that such DDM models provide a successful fit to the Fermi-LAT data. Our conclusions are then presented in Sect. V, where we also discuss the potential implications of energy duality for other astrophysical gamma-ray signals which might be observed in the future. Finally, an Appendix contains a derivation of certain results presented in the text.

## II. ENERGY DUALITY AND THE GALACTIC-CENTER EXCESS

As discussed in the Introduction, there is evidence of an unexplained gamma-ray excess from the GC in the Fermi-LAT data near 1 GeV that may be due to DM annihilations or decays. We consider the analysis in Ref. [9], in which the gamma-ray excess has been identified out to at least  $10^\circ$  from the GC. The authors of Ref. [9] fit the Fermi-LAT data to background templates consisting of the Galactic and extragalactic diffuse emission and the Fermi Bubbles. They also include a potential signal template for dark-matter annihilations. This latter contribution may be written in terms of a differential-flux contribution from dark-matter annihilation. In a single-particle dark-matter scenario, this flux  $\mathcal{F}$  may be written in the form

$$\mathcal{F} \equiv \frac{d^2\Phi}{dE_\gamma d\Omega} = \frac{\mathcal{J} \langle\sigma v\rangle dN_\gamma}{4\pi 4m^2 dE_\gamma}, \quad (2.1)$$

where  $m$  is the mass of the DM particle and  $\langle\sigma v\rangle$  is its velocity-averaged annihilation cross section. Here  $\mathcal{J} = \int d\ell \rho^2$ , where  $\rho$  is the dark-matter energy density and the integral is along the line of sight. Since the only non-trivial angular dependence for  $\mathcal{F}$  arises from  $\mathcal{J}$ , we may replace  $\mathcal{J}$  in Eq. (2.1) by its angular average  $\bar{\mathcal{J}}$  over a relevant angle  $\Delta\Omega$  on the sky, where

$$\bar{\mathcal{J}} \equiv \frac{1}{\Delta\Omega} \int_{\Delta\Omega} d\Omega \mathcal{J}. \quad (2.2)$$

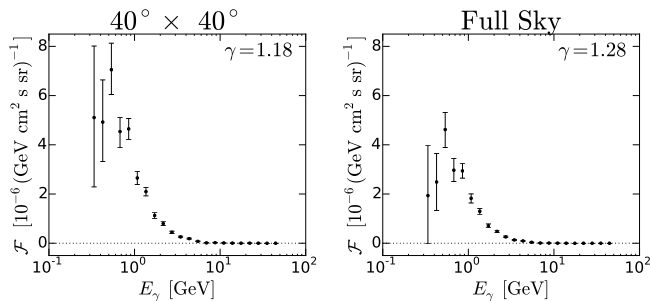


FIG. 1: The observed GC flux excess  $\mathcal{F}$ . The data points and the associated error bars are extracted from Ref. [9], while the values of  $\gamma$  indicated in each panel are the best-fit inner slopes of the generalized NFW profile in Eq. (2.4). Note that these two panels correspond to different regions on the sky and thus correspond to different values of  $\overline{\mathcal{J}}$ .

We then find that

$$\frac{d\Phi}{dE_\gamma} = \frac{J}{4\pi} \frac{\langle\sigma v\rangle}{4m^2} \frac{dN_\gamma}{dE_\gamma} \quad (2.3)$$

where  $J \equiv (\Delta\Omega)\overline{\mathcal{J}}$ . In writing Eq. (2.1) we have assumed that the dark-matter particle is distinct from the antiparticle; if the particle and antiparticle are identical, the flux is rescaled by a factor of 2. The energy density  $\rho$  is assumed to follow a generalized Navarro-Frenk-White (NFW) halo profile [44, 45]

$$\rho(r) = \rho_0 \frac{(r/r_s)^{-\gamma}}{(1+r/r_s)^{3-\gamma}}, \quad (2.4)$$

where  $\rho_0 \simeq 0.4 \text{ GeV/cm}^3$  is the local DM density at  $r \simeq 8.5 \text{ kpc}$  and where  $r_s = 20 \text{ kpc}$  is the scale radius. It is then found [9] that inclusion of this additional template with an inner-profile slope in the range  $\gamma \approx 1.1\text{--}1.3$  significantly improves the overall fit, with the dark-matter contribution taking the form of a continuum bump which peaks around  $E_\gamma \sim 1 \text{ GeV}$ .

This dark-matter excess is shown in Fig. 1, where we plot the residuals of the differential photon flux obtained from the analysis in Ref. [9] of Fermi-LAT data from the GC. In this analysis, each photon is placed into one of 22 energy bins, equally spaced on a logarithmic scale between 0.3 and 50 GeV. We emphasize that the error bars in Fig. 1 are statistical only, and that there are also large astrophysical uncertainties from background modeling which are not shown. Note that there are two regions of interest (ROI) shown in Fig. 1: (i)  $40^\circ \times 40^\circ$  with  $1^\circ < |b| < 20^\circ$ ,  $|l| < 20^\circ$ ; and (ii) full sky with  $|b| > 1^\circ$ , where  $b$  and  $l$  are the Galactic latitude and longitude, respectively. The authors of Ref. [9] also perform an analysis for a third, smaller region  $|b| < 5^\circ$ ,  $|l| < 5^\circ$ , but there are fewer statistics and thus a larger energy binning for this ROI. As we later discuss, our model-independent analysis benefits from using regions with higher statistics.

Our interest in this paper is in the overall shape of this gamma-ray flux excess  $\mathcal{F}$ , and in particular the pos-

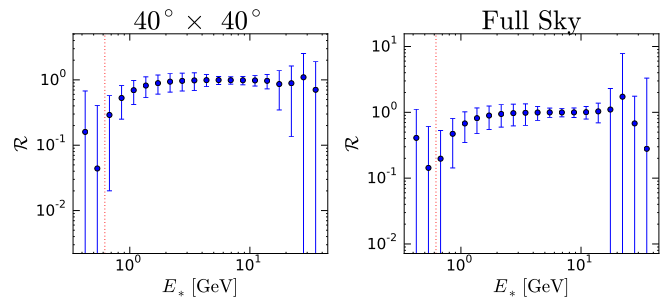


FIG. 2: Testing the energy-duality hypothesis for the Galactic-Center gamma-ray excess. We plot the asymmetric-to-symmetric ratio  $\mathcal{R}(n_*)$  in Eq. (2.5) as a function of the self-dual bin  $n_*$  containing  $E_*$ . We find that  $\mathcal{R}(n_*)$  is minimized at values near  $\mathcal{R}(n_*) \sim 10^{-1} - 10^{-2}$  for  $n_* = 3$ , signifying a reasonably good fit to a self-dual energy spectrum invariant under  $E_\gamma \rightarrow E_*^2/E_\gamma$  with a self-dual energy near  $E_* \sim 0.5 \text{ GeV}$ . The superimposed red dashed lines indicate the best-fit values for  $E_*$  taken from Fig. 5 for the DDM model in Sect. IV.

sibility that this spectrum exhibits an energy-duality invariance under  $E_\gamma \rightarrow E_*^2/E_\gamma$  for some  $E_*$ . Note that this is equivalent to  $x \rightarrow 1/x$  where  $x \equiv E_\gamma/E_*$ , or  $\log(x) \rightarrow -\log(x)$ . Thus, if this spectrum had an exact energy duality with  $E_*$  logarithmically centered inside a particular energy bin  $n_*$ , the plot in Fig. 1 would be completely symmetric on a logarithmic scale. In order to test this hypothesis, we quantify the extent to which this spectrum exhibits an energy duality by calculating the ratio of the asymmetric part versus the symmetric part of the spectrum as a function of the chosen reference bin  $n_*$  with respect to which these symmetries are calculated:

$$\mathcal{R}(n_*) \equiv \frac{\sum_{n=1}^{n_{\max}} |\mathcal{F}_{n_*+n} - \mathcal{F}_{n_*-n}|}{\sum_{n=1}^{n_{\max}} |\mathcal{F}_{n_*+n} + \mathcal{F}_{n_*-n}|}. \quad (2.5)$$

Here  $\mathcal{F}_m$  is that portion of the excess differential flux residing within the  $m^{\text{th}}$  energy bin, and  $n_{\max} \equiv \min(n_* - 1, 22 - n_*)$ . Our results are plotted in Fig. 2 for  $n_* = 2, \dots, 21$ . The value of  $n_*$  for which the asymmetric-to-symmetric flux ratio  $\mathcal{R}(n_*)$  is minimized indicates that the spectrum is most consistent with an energy duality for which the self-dual energy  $E_*$  is contained in that particular bin. Of course, we do not expect a perfect energy duality to be evident in the data. In particular, aside from statistical fluctuations, we do not expect a binned energy-dual spectrum to have a perfectly vanishing minimum asymmetric-to-symmetric ratio  $\mathcal{R}(n_*)$ , since an arbitrary binning will not logarithmically center a particular bin on  $E_*$ .

The results in Fig. 2 suggest that the GC excess may indeed be energy-dual with respect to the  $n_* = 3$  energy bin, corresponding to  $E_* \sim 0.5 \text{ GeV}$ . However, there are a few difficulties in confidently determining the value of  $E_*$  even if this energy duality does in fact exist. First, the energy binning prevents  $E_*$  from being determined

to within  $\sim 125$  MeV, although any particular energy-dual model may yield a more precise fit. Second, since the statistical variance in the differential flux at lower energies is large, the apparent energy duality may be an artifact of small statistics. Both better energy resolution and higher statistics are important in making a precise model-independent determination of  $E_*$ . (We note in this context that observations from, *e.g.*, GAMMA-400 [46] are expected to have a better resolution than the Fermi-LAT near 1 GeV.) Third, we see that there are only two bins below that which contains  $E_*$ . Thus data at even lower energies is needed in order to further test the energy duality from the higher-energy tail of the excess. Satellites that can probe the  $10 \text{ MeV} \lesssim E_\gamma \lesssim 1 \text{ GeV}$  energy range with sufficient resolution will be crucial in determining if the photon spectrum associated with the GC excess is indeed energy-dual. Finally, we again stress that error bars in Figs. 1 and 2 represent only statistical errors, and our discussion assumes that the systematic uncertainties (which we have been ignoring) do not ruin the energy duality. Indeed, all of these issues must be borne in mind when attempting to draw any robust conclusions from the shape of the GC gamma-ray spectrum extracted from current Fermi data. We shall return to these issues, and explore what such future experiments could do to foster a more robust claim for such a duality, in Sect. V.

Moreover, it should also be kept in mind that while annihilating/decaying dark matter provides one possible explanation for the excess observed in Fermi data, other explanations have been advanced as well. For example, a population of unresolved millisecond pulsars has been advanced as a plausible explanation for this excess [20, 21]. Alternatively, it has been pointed out that the GC excess can be explained in terms of leptonic cosmic-ray bursts of an astrophysical origin [47, 48], once the effects of standard steady-state diffusion [49] are properly taken into account.

Assuming the GC excess does have a dark-matter origin and is indeed energy-dual, it is also nevertheless possible that certain spectral features are masked due to the finite energy binning. As the photon energy approaches  $E_* \sim 0.5 \text{ GeV}$ , the spectrum has a single, sharp peak and falls off (nearly) monotonically above and below  $E_*$ . However, the spectrum could potentially consist of multiple overlapping peaks that cannot be resolved. Indeed, such a scenario could still be energy-dual. Alternatively, the spectrum could exhibit a plateau or smooth bump instead of a cuspy peak, as long as the critical size needed to distinguish between these possibilities is smaller than the size of the energy bins.

In the following sections, we shall assume that the GC gamma-ray excess indeed exhibits an energy-dual spectrum and discuss the physical implications that such an observation might have in terms of annihilating and/or decaying dark matter.

### III. BOOSTS AND BOXES: BUILDING AN ENERGY-DUAL SPECTRUM

In this section, we shall discuss the underlying kinematics that might lead to an energy-dual photon spectrum. Our focus shall be on energy-dual spectra which resemble a single continuum “bump” — *i.e.*, spectra whose magnitudes first rise as a function of energy and then fall.

#### A. Filling boxes through boosts

The most trivial example of a self-dual photon energy spectrum is a spectral line corresponding to monoenergetic photons with  $E_\gamma = E_*$ . Indeed, this spectrum is self-dual regardless of the spatial orientations of the various photon momenta, and is thus self-dual if the photon momenta are distributed isotropically. However, what is perhaps less trivial is that the energy spectrum of such photons remains self-dual even if such photons are boosted relative to the lab frame in which the photon energies are measured. Indeed, all that is required is that the photons continue to be distributed isotropically in the boosted frame. To see this, let us imagine that a given photon with energy  $E_*$  is boosted with a velocity  $\beta$ , with an angle  $\theta$  between the photon momentum and the boost direction. In the lab frame, the corresponding photon energy will be given by

$$E_\gamma = \gamma E_* (1 + \beta \cos \theta) \quad (3.1)$$

where  $\gamma = (1 - \beta^2)^{-1/2}$  is the usual relativistic factor. Since the probability distribution for these photons is assumed to be isotropic in the boosted frame, all values of  $\cos \theta$  are sampled with equal probability. Thus, the resulting photon spectrum will fill out a spectral “box” in energy space stretching between  $E_\gamma^\pm \equiv \gamma E_* (1 \pm \beta)$ . It is easy to verify that such a spectrum continues to be duality invariant. For  $\beta = 0$  (vanishing boost), this box collapses to the original spectral line at  $E_\gamma = E_*$ . However for non-zero boosts this spectral line expands in a self-dual way to form a box of width

$$\Delta E \equiv E_\gamma^+ - E_\gamma^- = 2\gamma\beta E_* , \quad (3.2)$$

logarithmically centered at  $E_* = \sqrt{E_\gamma^- E_\gamma^+}$ .

Such a kinematics is easy to realize if our monoenergetic photons are isotropically emitted through the decay of a massive particle  $\phi$  with momentum  $p_\phi$ . In this case the momentum  $p_\phi$  produces the required boost, whereupon we can identify  $\gamma = E_\phi/m_\phi$  and  $\gamma\beta = p_\phi/m_\phi$ . The width of the resulting spectral box is then given by

$$\Delta E = 2E_* \frac{p_\phi}{m_\phi} = \frac{2E_*}{m_\phi} \sqrt{E_\phi^2 - m_\phi^2} . \quad (3.3)$$

This width vanishes in the zero-boost limit  $E_\phi \rightarrow m_\phi$ . Otherwise, the width of this box grows as a function of

$E_\phi$  and encompasses an ever-increasing range of energies. We can further ensure that the photons emitted through such a  $\phi$  decay will be isotropic if  $\phi$  is spinless or at least unpolarized; likewise such photons will be mono-energetic in the  $\phi$  rest frame if this is a two-body decay, *i.e.*,  $\phi \rightarrow \gamma Y$  for some particle  $Y$ . In this case we find that

$$E_* = \frac{m_\phi^2 - m_Y^2}{2m_\phi}. \quad (3.4)$$

Given this setup, we may ask what minimum boost (*i.e.*, what minimum value of  $E_\phi$ ) is required in order for our resulting photon spectrum in the lab frame to include a given energy  $E_\gamma$ . Clearly, this is tantamount to determining the minimum value of  $E_\phi$  for which  $E_\gamma^- \leq E_\gamma \leq E_\gamma^+$ . Solving these inequalities, we find that we must have

$$E_\phi \geq \frac{m_\phi}{2} \left( x + \frac{1}{x} \right) \quad \text{where } x \equiv \frac{E_\gamma}{E_*}. \quad (3.5)$$

This result displays the expected energy-duality invariance under  $x \rightarrow 1/x$ , and thus holds regardless of whether  $E_\gamma < E_*$  or  $E_\gamma > E_*$ . Moreover, as expected, we see that no boost at all is required if  $E_\gamma = E_*$ : indeed for  $x = 1$  we find from Eq. (3.5) that any  $E_\phi \geq m_\phi$  will suffice.

### B. Stacking boxes to build an energy-dual spectrum

Thus far, we have seen that any massive particle  $\phi$  that decays isotropically into a two-body final state including at least one photon will lead to a self-dual “box”-like photon energy spectrum. However, given this, it is not hard to imagine how we might realize a given self-dual “bump”-like energy spectrum: we simply stack different boxes on top of each other, utilizing boxes with suitably chosen widths and heights. Indeed, any self-dual bump-like spectrum can be decomposed into a collection of such boxes, in much the same way as any periodic curve can be Fourier-decomposed into cosines and sines of different frequencies. This stacking procedure is illustrated in Fig. 3.

At a physical level, this procedure may be interpreted kinematically as follows. As we have seen, a given box represents the energy spectrum of a photon emerging from the two-body decay of a massive particle  $\phi$  with a given boost energy  $E_\phi$ : the width of the box corresponds to the boost energy  $E_\phi$  via Eq. (3.3), while the height of the box is determined by the (differential) number of such  $\phi$  particles with that boost energy. A given collection of boxes with various widths and heights therefore corresponds to a specific (differential) number  $N_\phi$  of  $\phi$  particles as a function of boost energy  $E_\phi$ .

Mathematically, if our bump-like photon spectrum corresponds to a differential photon number  $dN_\gamma/dE_\gamma$ , the

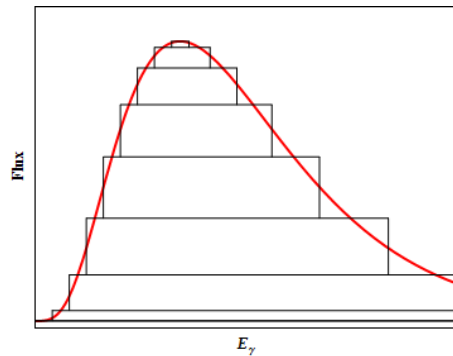


FIG. 3: Stacking boxes (black outlines) to build a self-dual photon energy spectrum (red curve). By stacking self-dual boxes of suitably chosen widths and heights, we can reproduce any bump-like self-dual photon energy spectrum. As described in the text, a given collection of boxes with various widths and heights corresponds to a specific differential number  $dN_\phi/dE_\phi$  of parent  $\phi$  particles with different boost energies  $E_\phi$ . It is these parent particles whose two-body decays produce the photons whose bump-like energy spectrum we are modeling.

process of superposition in Fig. 3 corresponds to writing

$$\frac{dN_\gamma}{dE_\gamma} = n_\gamma \int_{m_\phi}^{\infty} dE_\phi \frac{dN_\phi}{dE_\phi} \frac{\Theta(E_\gamma^+ - E_\gamma)\Theta(E_\gamma - E_\gamma^-)}{2E_* p_\phi / m_\phi} \quad (3.6)$$

where  $dN_\phi/dE_\phi$  represents the corresponding differential number of decaying  $\phi$  particles. Indeed, as described above, we may realize any self-dual function  $dN_\gamma/dE_\gamma$  in Eq. (3.6) through an appropriate choice of  $dN_\phi/dE_\phi$ , provided that  $dN_\gamma/dE_\gamma$  is truly “bump-like”, decreasing monotonically away from its maximum in either direction with no smaller peaks elsewhere. In Eq. (3.6), the Heaviside theta-functions in the numerator of the integrand enforce the upper and lower energy limits of each box, while the width  $\Delta E$  in the denominator provides a proper corresponding normalization. Finally, the quantity  $n_\gamma$  denotes the number of mono-energetic photons produced per  $\phi$  decay. For the process  $\phi \rightarrow \gamma Y$  we have  $n_\gamma = 1$  unless  $Y = \gamma$ , in which case  $n_\gamma = 2$ .

Note that Eq. (3.6) may equivalently be written as

$$\frac{dN_\gamma}{dx} = n_\gamma \int_{\frac{m_\phi}{2}(x+1/x)}^{\infty} dE_\phi \left[ \frac{dN_\phi}{dE_\phi} \frac{m_\phi}{2\sqrt{E_\phi^2 - m_\phi^2}} \right] \quad (3.7)$$

where  $x \equiv E_\gamma/E_*$  and where the lower limit of integration comes from Eq. (3.5). Of course, in writing these integrals we are assuming an essentially “continuous” collection of boxes, as would be required in order to produce a net photon energy spectrum which rises and falls smoothly compared with a corresponding detector resolution/binning. Note that the integral in Eq. (3.7) depends on  $x$  only through the lower limit of integration and the integrand is non-negative; thus,  $dN_\gamma/dx$  decreases as the lower limit of integration increases. However,  $x + 1/x$  is

minimized at  $x = 1$  and grows monotonically as  $x$  departs from 1 in either direction. Thus, the spectrum  $dN_\gamma/dx$  is maximized at  $x = 1$ , and decreases monotonically as  $x$  either increases or decreases away from this limit.

In stacking our boxes, it is interesting to distinguish between three distinct cases: those which lead to a cusp for  $dN_\gamma/dE_\gamma$  at the self-dual energy  $E_\gamma = E_*$ , those which lead to a smoothly rounded maximum, and those which lead to a flat plateau. These cases can be distinguished by examining the derivative of the differential photon number as we approach the self-dual energy  $E_*$ :

$$\left. \frac{d^2 N_\gamma}{dx^2} \right|_{x \rightarrow 1} = \text{sgn}(1-x) n_\gamma \frac{m_\phi}{2} \left. \frac{dN_\phi}{dE_\phi} \right|_{E_\phi \rightarrow m_\phi}. \quad (3.8)$$

Thus, if  $dN_\phi/dE_\phi$  is non-vanishing as  $E_\phi \rightarrow m_\phi$ , then the derivative of the spectrum is discontinuous, implying that  $dN_\gamma/dx$  has a cuspy peak at  $x = 1$  [40, 50]. By contrast, if  $dN_\phi/dE_\phi$  approaches zero smoothly as  $E_\phi \rightarrow m_\phi$ , then the peak is a smooth bump. However, if  $dN_\phi/dE_\phi$  vanishes below a threshold energy  $\bar{E} > m_\phi$ , then the photon spectrum exhibits a plateau along its maximum. In this case,  $dN_\gamma/dx$  is constant for  $x+1/x < 2\bar{E}/m_\phi$  [39, 40, 51]. Further discussions concerning these observations can be found in Refs. [40, 50, 52–55] within the context of collider phenomenology, and in Refs. [41, 51] within the context of gamma-ray astrophysics. Of course, while the current data describing the GC excess is consistent with a sharp peak, it is also consistent with a narrow plateau or smoothly rounded maximum, provided the width of the bump is less than the resolution of the binning.

We thus conclude that an energy-dual gamma-ray spectrum can easily emerge if these photons result from the isotropic two-body decays of massive particles  $\phi$  with a boost (or injection) spectrum  $dN_\phi/dE_\phi$ . In such cases the peak (or center of a plateau or smooth bump region) of our photon distribution determines  $E_*$ , while the spectral shape encodes the boost (or injection) spectrum  $dN_\phi/dE_\phi$ . Our remaining task, then, is to find a dark-matter model in which such an injection spectrum emerges naturally and is ultimately consistent with the GC excess.

#### IV. DYNAMICAL DARK MATTER AND THE GALACTIC-CENTER EXCESS

In principle, one can imagine many models of dark-sector physics in which dark-matter annihilations or decays produce a particle  $\phi$  whose subsequent decays produce the photons which are observed emanating from the Galactic Center. Likewise, there are many possibilities which give rise to a non-trivial injection spectrum  $dN_\phi/dE_\phi$  for these intermediary particles. For example, dark-matter decays or annihilations involving  $N$ -body final states with  $N > 2$  will lead to a non-trivial injection spectrum  $dN_\phi/dE_\phi$  if  $\phi$  is one of the resulting decay products. Other more complicated scenarios are also possible.

One particularly simple possibility, however, is to imagine that each of the “boxes” discussed in Sect. III corresponds to a different dark-matter particle  $\chi_n$  in the dark sector. Each  $\chi_n$  can then decay or annihilate, producing a pair of intermediary particles  $\phi$  which subsequently decay into two photons. This kinematics is sketched in Fig. 4. In the limit in which each  $\chi_n$  is non-relativistic with respect to the lab (observer) frame, the intermediaries  $\phi$  resulting from each such annihilation or decay will be generated with a fixed boost whose magnitude depends on the mass of  $\chi_n$ . Thus, if we wish to construct dark-matter models based on the kinematic configurations shown in Fig. 4, we are naturally led to consider dark sectors comprising different dark-matter particles  $\chi_n$  of different masses.

Remarkably, this is precisely one of the ingredients of the Dynamical Dark Matter (DDM) framework [42, 43]. In general, DDM models contain multiple dark-matter components which together form an ensemble whose phenomenological viability is the result of a balancing between decay widths and relic abundances across the ensemble. If the mass splitting between the ensemble components is smaller than the energy resolution of the detector in question, the boost distribution of the intermediary particles  $\phi$  appears continuous and thus the resulting photon spectrum appears as a continuum bump. A similar idea has been adopted in Ref. [56] within the context of MeV-range gamma-ray detection experiments.

#### A. Constructing a DDM model

Towards this end, we therefore consider a DDM model in which a (potentially) large number of DM components  $\chi_n$  form a dark-matter ensemble. We label the DDM components by the index  $n = 0, \dots, N$  in order of increasing mass. We assume that each  $\chi_n$  has a relic abundance  $\Omega_n$  such that the ensemble as a whole carries the observed total dark-matter relic abundance. Indeed, such DDM ensembles are realized in various well-motivated physics models beyond the SM, including scenarios with extra spacetime dimensions [42, 43, 57], confining hidden-sector gauge groups [58], large spontaneously-broken symmetry groups [59, 60], and even certain string configurations [58, 61].

In the case of DM annihilation, we consider a pair of  $\chi_n$ 's that annihilate to two  $\phi$ 's, each of which subsequently decays into two photons, as shown in Fig. 4(a). (For simplicity, we shall not consider the possibility of coannihilation by  $\chi_m$  and  $\chi_n$  where  $m \neq n$ .) As an example,  $\chi_n$  could be a Dirac fermion and  $\phi$  a singlet pseudoscalar (*e.g.*, a “dark pion” or an axion-like particle). A possible Lagrangian would then take the form

$$\mathcal{L}_{\text{ann}} \ni \sum_{n=0}^N \frac{c_n}{\Lambda} \bar{\chi}_n \chi_n \phi \phi + \frac{1}{f_\phi} \phi F_{\mu\nu} \tilde{F}^{\mu\nu}, \quad (4.1)$$

where  $\tilde{F}^{\mu\nu}$  denotes the usual dual field strength tensor,



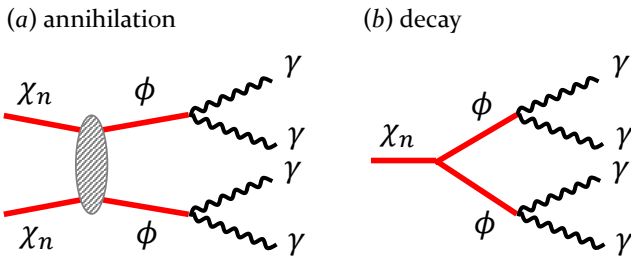


FIG. 4: Annihilating and decaying DDM model scenarios under consideration. The DDM components  $\chi_n$  annihilate or decay into the same intermediary particles  $\phi$ , which subsequently decay to two photons.

$\Lambda$  is the scale of the effective field theory that governs DM annihilations, and  $f_\phi$  is the symmetry-breaking scale that gives mass to the axion-like particle. The coupling  $c_n$  between  $\phi$  and  $\chi_n$  generically differs from component to component and so is also indexed by  $n$ .

In the case of DM decay, by contrast, we imagine a similar process in which a single  $\chi_n$  decays into two  $\phi$ 's, *i.e.*,  $\chi_n \rightarrow 2\phi \rightarrow 4\gamma$ , as shown in Fig. 4(b). One possible scenario involves a scalar  $\chi_n$  that decays into a pair of singlet pseudoscalar  $\phi$  particles. The possible corresponding Lagrangian would then take the form

$$\mathcal{L}_{\text{dec}} \ni \sum_{n=0}^N c'_n M \chi_n \phi \phi + \frac{1}{f_\phi} \phi F_{\mu\nu} \tilde{F}^{\mu\nu}, \quad (4.2)$$

where  $M$  is an associated mass scale which depends on the details of the underlying model. As in the annihilation case, the coupling  $c'_n$  between  $\phi$  and  $\chi_n$  can be different for different components.

However, this is not all. DDM models do not merely have a random assortment of dark-matter components — these components must also have properties such as masses, abundances, and decay widths which obey specific *scaling relations*. These scaling relations emerge naturally from a variety of underlying DDM constructions [42, 43, 57–60]. The question that remains, then, is not merely whether there exists a non-trivial intermediary injection spectrum  $dN_\phi/dE_\phi$  that can fit the GC excess, *but whether this injection spectrum is also consistent with an underlying dark sector whose individual components exhibit scaling relations of the sort DDM assumes*. Only this would be the true test of an underlying DDM-based origin for the GC excess.

We therefore consider how physical quantities such as the relic abundances, cross sections, and decay widths associated with our dark-matter components  $\chi_n$  vary across the ensemble. In general, these quantities can be parametrized in terms of the corresponding masses  $m_n$ . As a result, the photon flux  $\Phi_n$  associated with  $\chi_n$  (resulting from either decay or annihilation) will also depend on the mass  $m_n$ . For concreteness, just as in Ref. [56], we shall consider the case where  $\Phi_n$  scales with  $m_n$  ac-

ording to a simple power law of the form

$$\Phi_n = \Phi_0 \left( \frac{m_n}{m_0} \right)^\xi = \Phi_0 \left( \frac{\sqrt{s_n}}{\sqrt{s_0}} \right)^\xi, \quad (4.3)$$

where the scaling exponent  $\xi$  is taken to be a free parameter. Note that we replace the masses in Eq. (4.3) by the center-of-mass (CM) energies  $\sqrt{s_n}$  in order that our results are expressed in a form applicable to both the annihilation and decay scenarios. In the non-relativistic regime,  $\sqrt{s_n}$  is equal to  $2m_n$  or  $m_n$  for annihilating or decaying DM models, respectively.

In most DDM models, the masses  $m_n$  can typically be parametrized in terms of the mass  $m_0$  of the lightest DDM component, a mass-splitting parameter  $\Delta m$ , and a scaling exponent  $\delta$ :

$$m_n = m_0 + n^\delta \Delta m. \quad (4.4)$$

The CM energy gap between neighboring DM states, *i.e.*,  $\Delta(\sqrt{s_n}) \equiv \sqrt{s_{n+1}} - \sqrt{s_n}$ , is simply given by

$$\Delta(\sqrt{s_n}) = \begin{cases} 2[(n+1)^\delta - n^\delta] \Delta m & \text{for annihilation} \\ [(n+1)^\delta - n^\delta] \Delta m & \text{for decay,} \end{cases} \quad (4.5)$$

which is valid up to  $n = N - 1$ . In this paper, we shall choose  $\delta = 1$ , as arises in cases where the DDM ensemble are the states in a Kaluza-Klein tower. With this choice of  $\delta$ , the mass spectrum of the DDM ensemble has a uniform spacing. This allows us to write the CM energy gap as  $\Delta(\sqrt{s})$  and thereby eliminate the unnecessary subscript  $n$ . Indeed, we find that  $\Delta(\sqrt{s})$  is  $2\Delta m$  for annihilation and  $\Delta m$  for decay.

Given this scaling behavior, we can now calculate the differential photon number  $dN_\gamma/dE_\gamma$  corresponding to our DDM ensemble. To do this, we shall work in the continuum limit in which  $\Delta m \rightarrow 0$ . In this limit, we no longer have a discrete set of energies  $\sqrt{s_n}$ ; we instead have a continuous CM energy  $\sqrt{s}$  stretching between  $\sqrt{s_0}$  and  $\sqrt{s_N}$ . Indeed, we may replace sums  $\sum_{n=0}^N$  with integrals  $\int_{\sqrt{s_0}}^{\sqrt{s_N}} d\sqrt{s}/\Delta(\sqrt{s})$ . Likewise, we no longer have a discrete set of individual contributions  $\Phi_n$  to the total flux at different discrete values of  $\sqrt{s_n}$ ; we instead have a *function*  $\Phi(\sqrt{s})$  which describes the total flux emerging from an underlying dark-matter annihilaton or decay with CM energy  $\sqrt{s}$ . In other words, in this limit, Eq. (4.3) becomes

$$\Phi(\sqrt{s}) = \Phi_0 \left( \frac{\sqrt{s}}{\sqrt{s_0}} \right)^\xi. \quad (4.6)$$

Note that since  $\Phi(\sqrt{s})$  is not a *differential* flux, it carries no spectral information about the resulting photons. Rather, this quantity represents a particular contribution to the *total* gamma-ray flux.

While there are many ways in which we might calculate the total flux corresponding to our DDM ensemble, we shall here follow a somewhat quick and intuitive path

which is similar in spirit to the “stacking boxes” discussion above. A more rigorous derivation leading to the same result (and justifying its overall normalization) appears in the Appendix.

We shall assume that each ensemble constituent  $\chi_n$  annihilates or decays into a pair of  $\phi$  particles, each with energy  $E_\phi = \sqrt{s_n}/2$ , and that each such  $\phi$  particle in turn decays into a pair of photons. Thus, the differential number of  $\phi$  particles produced by dark-matter annihilation or decay with energy  $E_\phi$  is proportional to the total flux density at  $\sqrt{s} = 2E_\phi$ :

$$\frac{dN_\phi}{dE_\phi} \propto \Phi(2E_\phi). \quad (4.7)$$

Next, we recognize that for each ensemble component  $\chi_n$ , the corresponding contribution to  $dN_\phi/dE_\phi$  may be written as

$$\frac{dN_\phi^{(n)}}{dE_\phi} = 2 \delta(E_\phi - \sqrt{s_n}/2) \quad (4.8)$$

where the prefactor indicates that there are precisely two  $\phi$  particles produced from the annihilation/decay of each  $\chi_n$ . Thus, just as we stack boxes with appropriate heights in order to build our total spectrum as in Fig. 3, we can sum over all of the states in the ensemble with the appropriate weightings given in Eq. (4.7) in order to build our total “effective” differential number  $dN_\phi/dE_\phi$ :

$$\begin{aligned} \frac{dN_\phi}{dE_\phi} &\propto 2 \int_{\sqrt{s_0}}^{\sqrt{s_N}} \frac{d\sqrt{s}}{\Delta(\sqrt{s})} \left( \frac{\sqrt{s}}{\sqrt{s_0}} \right)^\xi \delta(E_\phi - \sqrt{s}/2) \\ &= \frac{4}{\Delta(\sqrt{s})} \left( \frac{2E_\phi}{\sqrt{s_0}} \right)^\xi \\ &\quad \times \Theta \left( \frac{\sqrt{s_N}}{2} - E_\phi \right) \Theta \left( E_\phi - \frac{\sqrt{s_0}}{2} \right). \end{aligned} \quad (4.9)$$

Indeed, this is precisely the injection spectrum  $dN_\phi/dE_\phi$  which has appeared throughout the main body of this paper thus far. This notion of an “effective”  $dN_\phi/dE_\phi$  will be discussed more precisely in the Appendix.

Note that the behavior of the injection spectrum  $dN_\phi/dE_\phi$  as  $E_\phi \rightarrow m_\phi$  depends on  $\xi$  and  $s_0$ . For  $s_0 > 4m_\phi^2$ , this injection spectrum is identically zero in the range  $m_\phi < E_\phi < \sqrt{s_0}/2$ , yielding a plateau-like maximum in the photon spectrum. On the other hand, for  $s_0 \sim 4m_\phi^2$ , the injection spectrum decreases as  $E_\phi \rightarrow m_\phi$  for positive  $\xi$ , yielding only a mild discontinuity in the derivative of the resulting photon spectrum near its maximum. For negative  $\xi$ , however, one would find a sharper peak.

Evaluating the photon spectrum that follows from this result for  $dN_\phi/dE_\phi$  is now simply a matter of substituting Eq. (4.9) into Eq. (3.7) with  $n_\gamma = 2$ . We thus obtain

$$\begin{aligned} \frac{dN_\gamma}{dx} &\propto \frac{2m_\phi}{\Delta(\sqrt{s})} \left( \frac{2m_\phi}{\sqrt{s_0}} \right)^\xi \\ &\quad \times \left[ B_{z_+} \left( -\frac{\xi}{2}, \frac{1}{2} \right) - B_{z_-} \left( -\frac{\xi}{2}, \frac{1}{2} \right) \right], \end{aligned} \quad (4.10)$$

where  $B_z(a, b)$  denotes the incomplete Euler beta function and where

$$\begin{aligned} z_+ &\equiv \max \left( \frac{4m_\phi^2}{s_N}, \min \left[ \frac{4m_\phi^2}{s_0}, \frac{4}{(x+1/x)^2} \right] \right), \\ z_- &\equiv \frac{4m_\phi^2}{s_N}. \end{aligned} \quad (4.11)$$

Our final step is to convert this expression for  $dN_\gamma/dx$  into a total differential flux  $d\Phi/dE_\gamma$ . However, in terms of the total “effective”  $dN_\gamma/dE_\gamma$  given in Eq. (4.10), we know that

$$\frac{d\Phi/dE_\gamma}{\Phi_0} = \frac{dN_\gamma/dE_\gamma}{N_\gamma^{(0)}} = \frac{dN_\gamma/dE_\gamma}{4}. \quad (4.12)$$

It then follows that

$$\frac{d\Phi}{dE_\gamma} = \frac{\Phi_0}{4} \frac{dN_\gamma}{dE_\gamma} = \frac{\Phi_0}{4E_*} \frac{dN_\gamma}{dx}, \quad (4.13)$$

where  $dN_\gamma/dx$  is given in Eq. (4.10).

The result in Eq. (4.13) is sufficient for understanding the shape of the overall photon spectrum. The normalization of this spectrum nevertheless remains unfixed because of the unknown normalization in Eq. (4.10). In general, the derivation we have provided is not capable of determining the correct normalization. However, given the prefactors already present in Eq. (4.10), we shall see in the Appendix that the remaining constant of proportionality in Eq. (4.10) is actually equal to one. Thus, in what follows, we shall feel free to replace the proportionality sign in Eq. (4.10) with an equals sign.

## B. Fitting the observed excess

Given the expression in Eq. (4.13) for the differential flux predicted by our DDM model, we can now perform a fit to the spectrum of the GC excess observed in the Fermi-LAT data. Note that the data reported in Ref. [9] is actually quoted in terms of the rescaled differential flux  $E_\gamma^2 d^2\Phi/(dE_\gamma d\Omega) \equiv E_\gamma^2 \mathcal{F}$ . Thus, putting the pieces together, we shall therefore fit this data to the predicted DDM template function

$$\begin{aligned} E_\gamma^2 \mathcal{F} &= \frac{E_\gamma^2}{\Delta\Omega} \Xi \left( \frac{4E_*}{\sqrt{s_0}} \right)^\xi \\ &\quad \times \left[ B_{z_+} \left( -\frac{\xi}{2}, \frac{1}{2} \right) - B_{z_-} \left( -\frac{\xi}{2}, \frac{1}{2} \right) \right], \end{aligned} \quad (4.14)$$

where

$$\begin{aligned} z_+ &\equiv \max \left( \frac{16E_*^2}{s_N}, \min \left[ \frac{16E_*^2}{s_0}, \frac{4}{(E_\gamma/E_* + E_*/E_\gamma)^2} \right] \right) \\ z_- &\equiv \frac{16E_*^2}{s_N} \end{aligned} \quad (4.15)$$



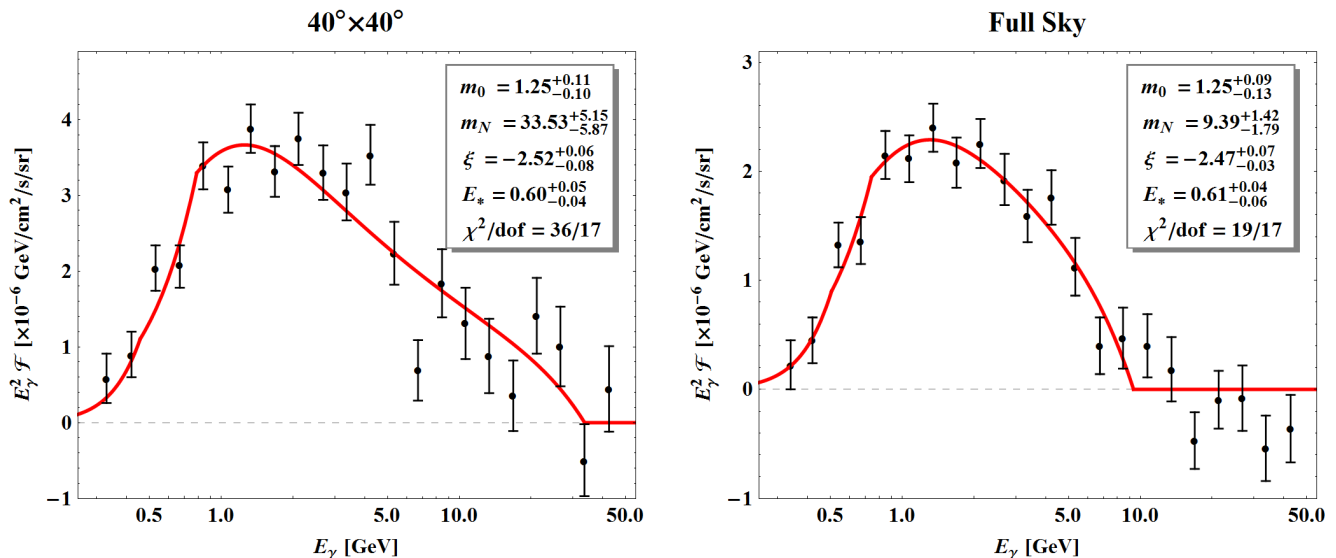


FIG. 5: The GC photon-excess spectra (black dots and error bars) extracted from Ref. [9], corresponding to ROI's (i) and (ii) for the left and right panels respectively, with the best-fit DDM flux superimposed in red. Input parameters for these best-fit curves are also shown in each panel, with the best-fit values for  $m_0$ ,  $m_N$ , and  $E_*$  quoted in GeV. These results indicate that our DDM model is successful in modelling the GC photon flux excess.

and where

$$\Xi \equiv \frac{\Phi_0}{\Delta(\sqrt{s})}. \quad (4.16)$$

Note that within this template we have replaced  $m_\phi$  in favor of the self-dual energy  $E_*$ . Moreover, because it provides a better fit to the spatial morphology of the excess, we shall focus on the annihilating dark-matter case, for which  $\sqrt{s_n} = 2m_n$ . Thus, we take  $\{m_0, m_N, \xi, E_*, \Xi\}$  as the five free parameters to which we perform our fit. Since the first four parameters describe the underlying particle-physics model, we would expect similar best-fit values to emerge for both ROI's. By contrast, the normalization factor  $\Xi$  depends not only on our specific particle-physics model but also on astrophysical information about the particular ROI — information encapsulated by the corresponding  $\mathcal{J}$ -factor which is implicit within  $\Phi_0$ . For this reason, the best-fit values of  $\Xi$  for our two ROI's need not be the same as each other.

In our analysis of the data for both ROI's, we perform our fits using the standard  $\chi^2$  statistic as our measure of goodness of fit. Our best-fit results for ROI (i) and ROI (ii) are displayed in the left and right panels of Fig. 5, respectively. The corresponding central values (black dots) for the gamma-ray flux in each bin are also shown in each panel, along with their associated error bars. The results shown in Fig. 5 indicate that our signal model reproduces the observational data for both ROI's rather well. Indeed, the  $\chi^2$  values for the fits performed on the data from ROI (i) and ROI (ii) are 36 and 19, respectively, with 17 degrees of freedom in each case (as there are 22 data points for each of our five-parameter fits). These numbers indicate that this DDM scenario is indeed successful in accounting for the GC excess.

The best-fit values for the parameters  $m_0$ ,  $m_N$ ,  $\xi$ , and  $E_*$  are shown in Fig. 5, with the first, second, and fourth of these quantities quoted in GeV. All of the reported errors are given at the 68% confidence level. We also find that

$$\Xi = \begin{cases} 1.81^{+0.15}_{-0.17} \times 10^{-6} \text{ (GeV cm}^2 \text{ s)}^{-1} & \text{for ROI (i)} \\ 30.26^{+2.80}_{-2.85} \times 10^{-6} \text{ (GeV cm}^2 \text{ s)}^{-1} & \text{for ROI (ii)}. \end{cases} \quad (4.17)$$

With the exception of  $m_N$ , we see that all of the model parameters measured for both ROI's are in good agreement with each other. This indicates that the shape of the excess does not change appreciably with the ROI and that our energy-dual scenario works well for both ROI's.

The mismatch in the  $m_N$  measurement is not surprising because only the upper and lower endpoints of the energy spectrum (*i.e.*, the horizontal edges of the widest box) are sensitive to  $m_N$ , and it is precisely here where the signal statistics are relatively poor. An over- or under-estimate of the foreground/background flux could therefore easily shift both endpoints rather substantially. Likewise, the best-fit values for  $E_*$  for each ROI, while consistent with each other, do not quite agree with the results of the model-independent analysis in Sect. II. However, as discussed above, the choice of energy-binning scheme may skew the model-independent results, as  $E_*$  does not have to lie at the center of a given energy bin. If this type of DDM scenario is realized in nature, one would expect the best-fit values for  $E_*$  from the two analyses to more closely coincide as more data is acquired and as the energy resolution of the detector is improved.

Finally, we observe that general features of our best-fit DDM models coincide nicely with the observed data.

As pointed out at the end of Sect. II, the observed data is consistent with a relatively sharp peak in the photon spectrum near the global maximum — a result which suggests that the injection spectrum  $dN_\phi/dE_\phi$  of the intermediary particle  $\phi$  remains non-zero as  $E_\phi \rightarrow m_\phi$ . Furthermore, the rapidly falling nature of the photon energy spectrum, as shown in Fig. 1, suggests that the injection spectrum of  $\phi$  should fall quickly as  $E_\phi/m_\phi$  increases. In typical examples, the injection spectrum of  $\phi$  particles produced from the annihilation/decay of a DDM ensemble typically follows a power law, as in Eq. (4.9). One would therefore expect that the best fit to the Fermi-LAT data would arise from a falling power law (*i.e.*, from a negative scaling exponent  $\xi < 0$ ). The results obtained in our fit coincide with this expectation.

## V. CONCLUSIONS

The possibility that the excess in the flux of gamma rays emanating from the vicinity of the GC is the result of annihilating or decaying dark matter is an intriguing one. If dark matter is indeed responsible for this excess, one pressing question is what, if anything, we can learn about the properties of the dark sector from the spectral information associated with that excess. Dark-matter models of the gamma-ray excess typically rely on complicated cascade mechanisms for photon production in order to reproduce the spectrum of the excess — mechanisms whose non-trivial kinematics obscures the connection between the properties of that spectrum and the properties of the dark-matter candidate.

In this paper, by contrast, we have considered an alternative dark-matter interpretation of the gamma-ray excess — one in which a more direct connection exists between the properties of the underlying dark sector and the spectral shape of the gamma-ray excess to which it gives rise. In particular, we have pointed out that the spectrum of the observed excess in the Fermi-LAT data is potentially invariant with respect to an energy duality transformation of the form  $E_\gamma \rightarrow E_*^2/E_\gamma$  for a self-dual energy  $E_* \sim \mathcal{O}(1 \text{ GeV})$ . Motivated by this observation, we have presented a broad class of physical scenarios wherein such an energy self-duality is realized. In these scenarios, dark-matter annihilation/decay produces a non-trivial injection spectrum  $dN_\phi/dE_\phi$  of intermediary particles  $\phi$ , each of which subsequently decays into a final state involving one or more photons which are mono-energetic and isotropically distributed in the  $\phi$  rest frame. We have also shown that an appropriate injection spectrum of  $\phi$  particles for describing the Fermi-LAT data is naturally realized within the context of the DDM framework.

It is clear that our scenario relies directly on the existence of a multi-component dark sector, as this is a primary ingredient of the DDM framework. The possibility of non-minimal dark sectors has received increasing attention because many DM models predicated upon

such sectors not only have non-trivial cosmological consequences (*e.g.*, “assisted freeze-out” [62]), but also often interesting phenomenological implications as well (*e.g.*, “boosted dark matter” [63–65] as well as collider, direct-detection, and indirect-detection signatures [66–70] that transcend those normally associated with traditional WIMP-like single-component dark-matter scenarios). Indeed, multi-component dark sectors can even give rise to enhanced complementarity relations which can be used to probe and constrain the parameter spaces of such models [71]. Thus, our explanation of the GC excess within the context of the DDM framework — if corroborated by future experiments — could provide an interesting window into the physics of the dark sector. Indeed, it would be interesting to study the cosmological and phenomenological implications of the particular set of DDM parameters obtained in our fit to the Fermi-LAT data.

It is also important to realize that our discussion of the energy duality of the photon spectrum under  $E_\gamma \rightarrow E_*^2/E_\gamma$  has a broad applicability that extends well beyond its application to the gamma-ray excess observed in the Fermi-LAT data. Indeed, this duality can be used as a tool for deciphering the origins of *any* generic continuum excess which might potentially be observed at future X-ray or gamma-ray facilities. As discussed in Sect. III, a broad range of spectral shapes can be realized within scenarios of the sort described above. In particular, any bump-like feature in the gamma-ray spectrum can be realized in such a scenario, provided

- the spectral feature is self-dual under the transformation  $E_\gamma \rightarrow E_*^2/E_\gamma$ ; and
- the spectral feature has a global maximum at  $E_\gamma = E_*$  and decreases monotonically as  $E_\gamma$  either increases or decreases away from  $E_*$ .

Moreover, we have shown that in scenarios of this sort, the shape of the spectral feature is directly correlated with the behavior of the intermediary injection spectrum at  $E_\phi = m_\phi$ . In particular, information about the kinematics of  $\phi$  production and decay is manifest in the behavior of  $dN_\gamma/dE_\gamma$  near its maximum:

- If  $dN_\phi/dE_\phi$  remains non-zero as  $E_\phi \rightarrow m_\phi$ , the photon spectrum will exhibit a cuspy peak at  $E_*$ .
- If  $dN_\phi/dE_\phi \rightarrow 0$  as  $E_\phi \rightarrow m_\phi$ , the photon spectrum will be smooth at  $E_*$ .
- If  $dN_\phi/dE_\phi$  vanishes below some threshold energy  $\bar{E} > m_\phi$ , the photon spectrum will exhibit a plateau around  $E_*$ .

Thus, an excess of photons emanating from any astrophysical source which possesses the above features not only lends itself to an interpretation in terms of our annihilating/decaying dark-matter scenario, but can also yield additional information about the properties of the underlying dark sector.

In general, an intermediary particle  $\phi$  which couples to photon pairs in the manner indicated in Eq. (4.2) will also couple to gluon pairs through an interaction term of the form  $\mathcal{L} \ni (c_g/f_\phi)\phi G_{\mu\nu}^a \tilde{G}^{\mu\nu a}$ , where  $G_{\mu\nu}^a$  is the gluon field-strength tensor and  $c_g$  is a dimensionless coefficient. Such an interaction term leads to additional, hadronic decay channels for  $\phi$ . The production of photons in association with these channels (through showering or from the decays of final-state hadrons) gives rise to an additional contribution to the differential photon flux. The production rate for these photons depends on the value of  $c_g$ , which is highly model-dependent. In this paper, for simplicity, we have assumed that  $c_g \ll 1$  and that this showering/hadron-decay contribution to  $d\Phi/dE_\gamma$  is therefore negligible.

It is nevertheless interesting to consider how our results would be modified in situations in which  $c_g \sim \mathcal{O}(1)$  and the showering/hadron-decay contribution is significant. In order to assess the impact of the showering/hadron-decay contribution on the overall photon signal spectrum from dark-matter annihilation in our DDM scenario, we begin by noting that this contribution, like the contribution from  $\phi \rightarrow \gamma\gamma$  decay, owes its shape both to the kinematics of photon production in the rest frame of a decaying  $\phi$  particle and to the spectrum of boosts imparted to the  $\phi$  particles by the DDM ensemble constituents. The spectrum of boosts is governed in large part by the scaling exponent  $\xi$ , which characterizes how the contribution to the production rate of  $\phi$  particles from an individual ensemble constituent  $\chi_n$  scales with  $m_n$  across the ensemble. As is evident from Fig. 5, the best-fit values for  $\xi$  for both of our ROI's are roughly  $\xi \approx -2.5$ , which implies that this contribution falls off rapidly with  $m_n$ . As a result, we find that the *collective* contribution to the production rate for secondary photons from ensemble constituents  $\chi_n$  with  $m_n$  above a few GeV is essentially negligible, even when  $c_g \sim \mathcal{O}(1)$ . Thus, the contribution to the overall signal flux from showering/hadron decay is expected to be significant only for  $E_\gamma \lesssim \mathcal{O}(1 \text{ GeV})$ .

The kinematics of photon production from showering/hadron-decay in the rest frame of the decaying intermediary has important ramifications as well. The primary parameter of interest here is  $m_\phi$ , our best-fit value for which is  $m_\phi \approx 1.2 \text{ GeV}$  for both ROI's. Since this is less than twice the proton mass, baryon-number conservation implies that final states consisting primarily of light mesons — and especially of pions — should dominate the partial width of  $\phi$  to hadrons. The dominant contribution to the secondary-photon spectrum at  $E_\gamma \sim \mathcal{O}(1 \text{ GeV})$  is therefore likely to be the contribution from on-shell  $\pi^0 \rightarrow \gamma\gamma$  decay. Photons produced in this way have their own distinctive kinematics. In particular, the energy spectrum associated with these photons manifests an energy duality of its own, with self-dual energy  $m_{\pi^0}/2$ . The presence of such a duality could be exploited in order to disentangle this contribution from the primary photon spectrum. In principle, one could significantly

reduce the contamination of the primary spectrum by subtracting off the contribution to the signal flux which is dual under  $E_\gamma \rightarrow m_{\pi^0}^2/(4E_\gamma)$ . Moreover, since the shape of this  $\pi^0$ -decay contribution to the secondary photon spectrum is correlated with the shape of the primary-photon spectrum, a comparison between these two contributions could provide additional evidence in support of a DDM origin for the GC excess. Indeed, this strategy has been successfully employed within the context of other, similar DDM scenarios [56]. Such an analysis would of course require improved data on the gamma-ray spectrum at energies  $E_\gamma \lesssim m_{\pi^0}/2$ . However, several proposals for instruments which would provide significant improvements in energy resolution within that energy range have been advanced [72, 73]. Thus, we see that “contamination” from the showering/hadron-decay contribution to the differential photon flux that arises in this DDM scenario when  $c_g \sim \mathcal{O}(1)$  may actually be an asset rather than a hurdle in the effort to distinguish this scenario from other models for the origin of this excess.

One final comment is in order. In particular, we stress that although the gamma-ray excess observed in the Fermi-LAT data is *consistent* with an energy duality of the kind we have discussed in this paper, there are significant uncertainties in the spectral shape of the excess which, at present, preclude any more definitive statements along these lines. These include not only statistical uncertainties, but also systematic uncertainties in the astrophysical foregrounds/backgrounds in the vicinity of the GC and uncertainties resulting from the energy resolution of the the Fermi-LAT instrument. Moreover, the preferred value for the self-dual energy  $E_* \sim \mathcal{O}(1 \text{ GeV})$  is very close to the lower limit of the energy range for which reliable data exists. As a result, current data does not yet permit us to distinguish between the annihilating/decaying dark-matter scenario we have described here and other possible explanations of the CG gamma-ray excess. However, there are new astronomical instruments, both planned and under consideration, which are far better equipped to investigate whether the gamma-ray spectrum from the GC indeed exhibits such an energy-duality. For example, GAMMA-400 is expected to have a better energy resolution than Fermi-LAT in the  $E_\gamma \sim 1 \text{ GeV}$  regime. A variety of instruments designed to study the gamma-ray spectrum in the  $10 \text{ MeV} \lesssim E_\gamma \lesssim 1 \text{ GeV}$  regime, such as ASTROGAM [73], have also recently been proposed, often with energy resolutions far superior to those of similar experiments past or present. High-statistics data from such experiments could potentially definitively rule out or else lend significant credence to our scenario. Indeed, this illustrates that even when an excess of photons observed at indirect-detection experiments has the form of a broad continuum bump, precision measurements of the spectral shape of this bump can prove crucial for our understanding of the underlying physics.

### Acknowledgments

We are grateful to Regina Caputo and Jeff Kost for useful discussions. We would also like to acknowledge the Center for Theoretical Underground Physics and Related Areas (CETUP\*) for hospitality and partial support during the 2016 Summer Program. KB and JK are supported in part by the National Science Foundation under CAREER Grant PHY-1250573, while KRD is supported in part by the Department of Energy under Grant DE-FG02-13ER41976 and by the National Science Foundation through its employee IR/D program. DK was supported in part by the U.S. Department of Energy under Grant DE-SC0010296 and is presently supported in part by the Korean Research Foundation (KRF) through the CERN-Korea Fellowship program. JCP is supported by the National Research Foundation of Korea (NRF-2013R1A1A2061561, 2016R1C1B2015225). The opinions and conclusions expressed herein are those of the authors, and do not represent any funding agencies.

### Appendix A: Calculating the Photon Flux of the DDM Model

In this Appendix we provide a rigorous calculation of the differential photon flux  $d\Phi/dE_\gamma$  corresponding to the DDM model introduced in Sect. IV A. This derivation will also confirm the normalization factors introduced in Eq. (4.14) and likewise clarify the meaning of the “effective” differential number  $dN_\phi/dE_\phi$  given in Eq. (4.9). By and large, our approach will generally follow that of Ref. [56].

We begin by noting that while the expression for the differential flux  $d\Phi/dE_\gamma$  in Eq. (2.3) is suitable for a single dark-matter candidate  $\chi$ , in multi-component contexts involving fields  $\chi_n$  with  $n = 0, 1, \dots, N$  this expression generalizes to take the form

$$\frac{d\Phi_n}{dE_\gamma} = \frac{J}{4\pi} \frac{\langle\sigma v\rangle_n}{4m_n^2} \frac{\Omega_n}{\Omega_{\text{tot}}} \frac{dN_\gamma^{(n)}}{dE_\gamma}. \quad (\text{A1})$$

Here  $\Phi_n$  and  $\Omega_n$  are respectively the flux contribution and cosmological abundance of  $\chi_n$ , with  $\Phi = \sum_{n=0}^N \Phi_n$  and  $\Omega_{\text{tot}} \equiv \sum_{n=0}^N \Omega_n$ . Likewise we observe that

$$\Phi_0 = \frac{J}{4\pi} \frac{\langle\sigma v\rangle_0}{4m_0^2} \frac{\Omega_0}{\Omega_{\text{tot}}} N_\gamma^{(0)} \quad (\text{A2})$$

where  $N_\gamma^{(0)} = 4$  is the number of photons produced through the annihilation of  $\chi_0$ . We can therefore write Eq. (A1) in the form

$$\frac{d\Phi_n}{dE_\gamma} = \frac{\Phi_0}{4} \left( \frac{m_0^2}{m_n^2} \frac{\Omega_n}{\Omega_0} \frac{\langle\sigma v\rangle_n}{\langle\sigma v\rangle_0} \right) \frac{dN_\gamma^{(n)}}{dE_\gamma}. \quad (\text{A3})$$

Given this, the DDM scaling behavior in Eq. (4.3) implies that the quantities within the parentheses in Eq. (A3)

each scale in such a way that this entire parenthesized factor is equal to  $(\sqrt{s_n}/\sqrt{s_0})^\xi$ . Summing over the modes of the ensemble and passing to the continuous integral form of the sum as described above Eq. (4.6) then yields

$$\frac{d\Phi}{dE_\gamma} = \frac{\Phi_0}{4\Delta(\sqrt{s})} \int_{\sqrt{s_0}}^{\sqrt{s_N}} d\sqrt{s} \left( \frac{\sqrt{s}}{\sqrt{s_0}} \right)^\xi \frac{dN_\gamma}{dE_\gamma}. \quad (\text{A4})$$

However, the differential photon number  $dN_\gamma/dE_\gamma$  is given in Eq. (3.7). Substituting this expression into Eq. (A4) and recognizing that  $E_* = m_\phi/2$ , we thus have

$$\begin{aligned} \frac{d\Phi}{dE_\gamma} &= \frac{\Phi_0}{2\Delta(\sqrt{s})} \int_{\sqrt{s_0}}^{\sqrt{s_N}} d\sqrt{s} \left( \frac{\sqrt{s}}{\sqrt{s_0}} \right)^\xi \\ &\times \int_{\frac{m_\phi}{2}(x+1/x)}^\infty dE_\phi \frac{1}{\sqrt{E_\phi^2 - m_\phi^2}} \frac{dN_\phi}{dE_\phi}. \end{aligned} \quad (\text{A5})$$

In Eq. (A5), the final quantity is the differential number  $dN_\phi/dE_\phi$ . Strictly speaking, this is given by

$$\frac{dN_\phi}{dE_\phi} = 2\delta(E_\phi - \sqrt{s}/2), \quad (\text{A6})$$

signifying that the annihilation of each dark-sector component with CM energy  $\sqrt{s}$  produces exactly two  $\phi$  particles with energies  $E_\phi = \sqrt{s}/2$ . However, it is possible to rewrite Eq. (A5) by exchanging the order of integrations, yielding

$$\begin{aligned} \frac{d\Phi}{dE_\gamma} &= \frac{\Phi_0}{2\Delta(\sqrt{s})} \int_{\frac{m_\phi}{2}(x+1/x)}^\infty dE_\phi \frac{1}{\sqrt{E_\phi^2 - m_\phi^2}} \\ &\times \int_{\sqrt{s_0}}^{\sqrt{s_N}} d\sqrt{s} \left( \frac{\sqrt{s}}{\sqrt{s_0}} \right)^\xi \frac{dN_\phi}{dE_\phi}. \end{aligned} \quad (\text{A7})$$

Given this, we may identify the entire quantity on the second line of Eq. (A7) as an “effective”  $dN_\phi/dE_\phi$ , one which combines not only the Dirac  $\delta$ -function contribution in Eq. (A6) but also the scaling factor  $(\sqrt{s}/\sqrt{s_0})^\xi$ . Indeed, this is precisely the quantity which was constructed in Eq. (4.9) and which (by abuse of notation) was casually denoted  $dN_\phi/dE_\phi$  throughout the body of the text. As such, it is this effective quantity which encodes not only the widths but also the heights of the stacked “boxes” in Fig. 3.

Eq. (A3) also affords us another way of interpreting this effective number  $dN_\phi/dE_\phi$ . In Eq. (A3), it is the quantity in parentheses which varies across the ensemble and which, in so doing, exhibits the DDM scaling behavior. However, for the purposes of calculating fluxes, we can equivalently imagine that the quantities within the parentheses in Eq. (A3) are actually constant, and that their scaling behavior has been absorbed into an effective differential number  $dN_\phi/dE_\phi$  instead. Indeed, it is precisely for these reasons that a simple relation such as that in Eq. (4.12) holds when written in terms of effective number densities.

Given the expression in Eq. (A7), evaluation of the flux  $d\Phi/dE_\gamma$  now proceeds directly. This then yields the

results listed in Sect. IV A and confirms the overall normalizations quoted there.

- 
- [1] L. Goodenough and D. Hooper, arXiv:0910.2998 [hep-ph].
- [2] D. Hooper and L. Goodenough, Phys. Lett. B **697**, 412 (2011) [arXiv:1010.2752 [hep-ph]].
- [3] D. Hooper and T. Linden, Phys. Rev. D **84**, 123005 (2011) [arXiv:1110.0006 [astro-ph.HE]].
- [4] K. N. Abazajian and M. Kaplinghat, Phys. Rev. D **86**, 083511 (2012) [Phys. Rev. D **87**, 129902 (2013)] [arXiv:1207.6047 [astro-ph.HE]].
- [5] D. Hooper and T. R. Slatyer, Phys. Dark Univ. **2**, 118 (2013) [arXiv:1302.6589 [astro-ph.HE]].
- [6] C. Gordon and O. Macias, Phys. Rev. D **88**, no. 8, 083521 (2013) [Phys. Rev. D **89**, no. 4, 049901 (2014)] [arXiv:1306.5725 [astro-ph.HE]].
- [7] W. C. Huang, A. Urbano and W. Xue, arXiv:1307.6862 [hep-ph].
- [8] K. N. Abazajian, N. Canac, S. Horiuchi and M. Kaplinghat, Phys. Rev. D **90**, no. 2, 023526 (2014) [arXiv:1402.4090 [astro-ph.HE]].
- [9] T. Daylan, D. P. Finkbeiner, D. Hooper, T. Linden, S. K. N. Portillo, N. L. Rodd and T. R. Slatyer, Phys. Dark Univ. **12**, 1 (2016) [arXiv:1402.6703 [astro-ph.HE]].
- [10] T. Lacroix, C. Boehm and J. Silk, Phys. Rev. D **90**, no. 4, 043508 (2014) [arXiv:1403.1987 [astro-ph.HE]].
- [11] B. Zhou, Y. F. Liang, X. Huang, X. Li, Y. Z. Fan, L. Feng and J. Chang, Phys. Rev. D **91**, no. 12, 123010 (2015) [arXiv:1406.6948 [astro-ph.HE]].
- [12] F. Calore, I. Cholis and C. Weniger, JCAP **1503**, 038 (2015) [arXiv:1409.0042 [astro-ph.CO]].
- [13] F. Calore, I. Cholis, C. McCabe and C. Weniger, Phys. Rev. D **91**, no. 6, 063003 (2015) [arXiv:1411.4647 [hep-ph]].
- [14] M. Ajello *et al.* [Fermi-LAT Collaboration], Astrophys. J. **819**, no. 1, 44 (2016) [arXiv:1511.02938 [astro-ph.HE]].
- [15] K. N. Abazajian, JCAP **1103**, 010 (2011) [arXiv:1011.4275 [astro-ph.HE]].
- [16] D. Hooper, I. Cholis, T. Linden, J. Siegal-Gaskins and T. Slatyer, Phys. Rev. D **88**, 083009 (2013) [arXiv:1305.0830 [astro-ph.HE]].
- [17] D. Hooper and T. Linden, [arXiv:1606.09250 [astro-ph.HE]].
- [18] T. Linden, E. Lovegrove and S. Profumo, Astrophys. J. **753**, 41 (2012) [arXiv:1203.3539 [astro-ph.HE]].
- [19] O. Macias and C. Gordon, Phys. Rev. D **89**, no. 6, 063515 (2014) [arXiv:1312.6671 [astro-ph.HE]].
- [20] R. Bartels, S. Krishnamurthy and C. Weniger, Phys. Rev. Lett. **116**, no. 5, 051102 (2016) [arXiv:1506.05104 [astro-ph.HE]].
- [21] S. K. Lee, M. Lisanti, B. R. Safdi, T. R. Slatyer and W. Xue, Phys. Rev. Lett. **116**, no. 5, 051103 (2016) [arXiv:1506.05124 [astro-ph.HE]].
- [22] M. Aguilar *et al.* [AMS Collaboration], Phys. Rev. Lett. **114**, 171103 (2015).
- [23] AMS-02 Collaboration, Talks at the ‘AMS Days at CERN’, 15-17 April (2015).
- [24] G. Giesen, M. Boudaud, Y. Genolini, V. Poulin, M. Cirelli, P. Salati and P. D. Serpico, JCAP **1509**, no. 09, 023 (2015) [arXiv:1504.04276 [astro-ph.HE]].
- [25] J. D. Ruiz-Alvarez, C. A. de S. Pires, F. S. Queiroz, D. Restrepo and P. S. Rodrigues da Silva, Phys. Rev. D **86**, 075011 (2012) [arXiv:1206.5779 [hep-ph]].
- [26] N. Okada and O. Seto, Phys. Rev. D **89**, no. 4, 043525 (2014) [arXiv:1310.5991 [hep-ph]].
- [27] K. P. Modak, D. Majumdar and S. Rakshit, JCAP **1503**, 011 (2015) [arXiv:1312.7488 [hep-ph]].
- [28] A. Alves, S. Profumo, F. S. Queiroz and W. Shepherd, Phys. Rev. D **90**, no. 11, 115003 (2014) [arXiv:1403.5027 [hep-ph]].
- [29] S. Ipek, D. McKeen and A. E. Nelson, Phys. Rev. D **90**, no. 5, 055021 (2014) [arXiv:1404.3716 [hep-ph]].
- [30] T. Mondal and T. Basak, Phys. Lett. B **744**, 208 (2015) [arXiv:1405.4877 [hep-ph]].
- [31] J. C. Park, S. C. Park and J. Kim, Phys. Lett. B **752**, 59 (2016) [arXiv:1505.04620 [hep-ph]].
- [32] B. Kyae and J. C. Park, Phys. Lett. B **732**, 373 (2014) [arXiv:1310.2284 [hep-ph]].
- [33] K. Kong and J. C. Park, Nucl. Phys. B **888**, 154 (2014) [arXiv:1404.3741 [hep-ph]].
- [34] C. Boehm, M. J. Dolan and C. McCabe, Phys. Rev. D **90**, no. 2, 023531 (2014) [arXiv:1404.4977 [hep-ph]].
- [35] P. Ko, W. I. Park and Y. Tang, JCAP **1409**, 013 (2014) [arXiv:1404.5257 [hep-ph]].
- [36] M. Abdullah, A. DiFranzo, A. Rajaraman, T. M. P. Tait, P. Tanedo and A. M. Wijangco, Phys. Rev. D **90**, no. 3, 035004 (2014) [arXiv:1404.6528 [hep-ph]].
- [37] A. Martin, J. Shelton and J. Unwin, Phys. Rev. D **90**, no. 10, 103513 (2014) [arXiv:1405.0272 [hep-ph]].
- [38] G. Elor, N. L. Rodd and T. R. Slatyer, Phys. Rev. D **91**, 103531 (2015) [arXiv:1503.01773 [hep-ph]].
- [39] F. W. Stecker, “Cosmic gamma rays,” *NASA Special Publication* **249** (1971).
- [40] K. Agashe, R. Franceschini and D. Kim, Phys. Rev. D **88**, no. 5, 057701 (2013) [arXiv:1209.0772 [hep-ph]].
- [41] D. Kim and J. C. Park, Phys. Dark Univ. **11**, 74 (2016) [arXiv:1507.07922 [hep-ph]].
- [42] K. R. Dienes and B. Thomas, Phys. Rev. D **85**, 083523 (2012) [arXiv:1106.4546 [hep-ph]].
- [43] K. R. Dienes and B. Thomas, Phys. Rev. D **85**, 083524 (2012) [arXiv:1107.0721 [hep-ph]].
- [44] J. F. Navarro, C. S. Frenk and S. D. M. White, Astrophys. J. **462**, 563 (1996) [astro-ph/9508025].
- [45] J. F. Navarro, C. S. Frenk and S. D. M. White, Astrophys. J. **490**, 493 (1997) [astro-ph/9611107].
- [46] A. M. Galper *et al.*, arXiv:1412.4239 [physics.ins-det].
- [47] J. Petrović, P. D. Serpico and G. Zaharijaš, JCAP **1410**, no. 10, 052 (2014) doi:10.1088/1475-7516/2014/10/052 [arXiv:1405.7928 [astro-ph.HE]].
- [48] I. Cholis, C. Evoli, F. Calore, T. Linden, C. Weniger and D. Hooper, JCAP **1512** (2015) no.12, 005 doi:10.1088/1475-7516/2015/12/005 [arXiv:1506.05119 [astro-ph.HE]].
- [49] D. Gaggero, M. Taoso, A. Urbano, M. Valli and P. Ullio, JCAP **1512**, no. 12, 056 (2015) doi:10.1088/1475-7516-2015-12-056, 10.1088/1475-7516/2015/12/056

- [arXiv:1507.06129 [astro-ph.HE]].
- [50] C. Y. Chen, H. Davoudiasl and D. Kim, Phys. Rev. D **89**, no. 9, 096007 (2014) [arXiv:1403.3399 [hep-ph]].
- [51] D. Kim and J. C. Park, Phys. Lett. B **750**, 552 (2015) [arXiv:1508.06640 [hep-ph]].
- [52] K. Agashe, R. Franceschini and D. Kim, JHEP **1411**, 059 (2014) [arXiv:1309.4776 [hep-ph]].
- [53] K. Agashe, R. Franceschini, D. Kim and K. Wardlow, Phys. Dark Univ. **2**, 72 (2013) [arXiv:1212.5230 [hep-ph]].
- [54] K. Agashe, R. Franceschini, D. Kim and K. Wardlow, arXiv:1503.03836 [hep-ph].
- [55] K. Agashe, R. Franceschini, S. Hong and D. Kim, arXiv:1512.02265 [hep-ph].
- [56] K. K. Boddy, K. R. Dienes, D. Kim, J. Kumar, J. C. Park and B. Thomas, Phys. Rev. D **94**, 095027 (2016) [arXiv:1606.07440 [hep-ph]].
- [57] K. R. Dienes and B. Thomas, Phys. Rev. D **86**, 055013 (2012) [arXiv:1203.1923 [hep-ph]].
- [58] K. R. Dienes, F. Huang, S. Su and B. Thomas, Phys. Rev. D **95**, 043526 (2017) [arXiv:1610.04112 [hep-ph]].
- [59] K. R. Dienes, J. Fennick, J. Kumar and B. Thomas, Phys. Rev. D **93**, 083506 (2016) [arXiv:1601.05094 [hep-ph]].
- [60] K. R. Dienes, J. Fennick, J. Kumar, and B. Thomas, to appear.
- [61] D. Chialva, P. S. B. Dev and A. Mazumdar, Phys. Rev. D **87**, no. 6, 063522 (2013) [arXiv:1211.0250 [hep-ph]].
- [62] G. Belanger and J. C. Park, JCAP **1203**, 038 (2012) [arXiv:1112.4491 [hep-ph]].
- [63] K. Agashe, Y. Cui, L. Necib and J. Thaler, JCAP **1410**, no. 10, 062 (2014) [arXiv:1405.7370 [hep-ph]].
- [64] J. Berger, Y. Cui and Y. Zhao, JCAP **1502**, no. 02, 005 (2015) [arXiv:1410.2246 [hep-ph]].
- [65] K. Kong, G. Mohlabeng and J. C. Park, Phys. Lett. B **743**, 256 (2015) [arXiv:1411.6632 [hep-ph]].
- [66] K. R. Dienes, S. Su and B. Thomas, Phys. Rev. D **86**, 054008 (2012) [arXiv:1204.4183 [hep-ph]].
- [67] K. R. Dienes, J. Kumar and B. Thomas, Phys. Rev. D **86**, 055016 (2012) [arXiv:1208.0336 [hep-ph]].
- [68] K. R. Dienes, J. Kumar and B. Thomas, Phys. Rev. D **88**, 103509 (2013) [arXiv:1306.2959 [hep-ph]].
- [69] K. R. Dienes, S. Su and B. Thomas, Phys. Rev. D **91**, 054002 (2015) [arXiv:1407.2606 [hep-ph]].
- [70] K. R. Dienes, J. Kost and B. Thomas, Phys. Rev. D **93**, 043540 (2016) [arXiv:1509.00470 [hep-ph]].
- [71] K. R. Dienes, J. Kumar, B. Thomas and D. Yaylali, Phys. Rev. Lett. **114**, 051301 (2015) [arXiv:1406.4868 [hep-ph]].
- [72] S. E. Boggs *et al.* [Larger ACT Collaboration], New Astron. Rev. **50**, 604 (2006) doi:10.1016/j.newar.2006.06.076 [astro-ph/0608532].
- [73] ASTROGAM Collaboration, <http://astrogam.iaps.inaf.it/index.html>.